A model of tension-induced fiber growth predicts white matter organization during brain folding

Kara Garcia (✉ karaellspermann@gmail.com)

  Indiana University School of Medicine   https://orcid.org/0000-0003-1325-0749

Xiaojie Wang

  Oregon Health & Science University

Christopher Kroenke

  Oregon Health & Science University   https://orcid.org/0000-0001-7398-3632

Article

1

2

3

4

5

6 **A model of tension-induced fiber growth predicts white matter organization during brain folding**

7

8 Kara E. Garcia[1,2,*], Xiaojie Wang[3,4], Christopher D. Kroenke[3,4]

9

10 1. Indiana University School of Medicine, Department of Radiology and Imaging Sciences, Evansville, IN
11 47715
12 2. Washington University in St. Louis, Department of Mechanical Engineering and Materials Science, St.
13 Louis, MO 63130
14 3. Oregon Health and Science University, Division of Neuroscience, Oregon National Primate Research
15 Center, Beaverton, OR, USA, 97006
16 4. Advanced Imaging Research Center, Oregon Health and Science University, Portland, OR, USA, 97239

17

18 *Corresponding author: karagarc@iu.edu

19

20

1 **<u>Abstract</u>**

2 The past decade has experienced renewed interest in the physical processes that fold the developing cerebral cortex.

3 Biomechanical models and experiments suggest that growth of the cortex, outpacing growth of underlying

4 subcortical tissue (prospective white matter), is sufficient to induce folding. However, current models do not explain

5 the well-established links between white matter organization and fold morphology, nor do they consider dramatic

6 subcortical remodeling that occurs during the period of folding. This study proposes a novel paradigm in which

7 cortical folding induces subcortical fiber growth and organization. Simulations incorporating stress-induced fiber

8 growth indicate that subcortical stresses resulting from folding are sufficient to induce stereotyped fiber organization

9 beneath gyri and sulci. Model predictions are supported by high-resolution *ex vivo* diffusion tensor imaging of the

10 developing rhesus macaque brain. Results provide support for the theory of cortical growth-induced folding and

11 indicate that mechanical feedback plays a significant role in brain connectivity.

1. Introduction

In gyrencephalic species, such as humans, several lines of evidence support a fundamental link between the structure of brain folds and the connectivity of underlying white matter. In clinical disorders such as epilepsy, autism, bipolar disorder, and schizophrenia, differences in both white matter organization and cortical folding have been reported[1-4]. In animal models, lesion experiments directed at specific axon fiber tracts have been shown to induce abnormal cortical morphology[5]. Furthermore, gyral and sulcal structure inherently influence the lengths of axons necessary to connect different regions of the cortex, such that cortical morphology and axonal "wiring length efficiency" are intrinsically linked[6]. However, the mechanistic relationship between white matter organization and cortical folding remains ill-defined.

Several hypotheses have been proposed to explain the role of developing white matter in cortical folding (Fig. 1). Over the period of cortical expansion and folding, the subplate (prospective white matter tissue between the cortical plate and outer fibrous layers) transforms from a loose arrangement of cell bodies, radial glial scaffolds, and neuronal processes, into a tightly organized, axon-rich tissue[7]. Thickness of the subplate has been correlated to both gyrification and complexity of cortico-cortical (association) fiber systems, and short association fibers have been reported to emerge around the time of gyrification[7-9]. Based on these observations, some researchers have proposed that the subplate actively pushes the cortex outward to form gyri[7-9], while others have proposed axons tether specific, highly connected regions[6] to direct folding. However, physical measurements performed in developing brain tissue found mechanical stresses inconsistent with both of these proposed theories[10].

In light of these stress measures, recent studies have focused on a third potential mechanism of folding, in which cortical expansion – constrained by slower growth of the underlying subplate – eventually leads to mechanical buckling or creasing[11-13]. Critically, biomechanical simulations of this process predict tissue stresses consistent with experimental observations[10]. Among these studies, several have proposed that the subplate behaves as a viscoelastic material, based evidence that the subplate contains axons and that axons generally lengthen in response to sustained stretch[14-16]. Using both closed-form solutions and finite element modeling, Bayly and colleagues[17] demonstrated that a viscoelastic subplate can produce normal brain folding, and that lissencephaly or polymicrogyria could be explained by a faster or slower viscoelastic response of the subplate relative to cortical growth rate. Expanding on this work, simulations by Holland and colleagues[18] illustrated how patterned subplate orientations could bias the

1   location and direction of buckling-induced folds. However, a limitation of both studies was the application of

2   viscoelasticity to all subcortical tissue, rather than considering separate contributions of specific cellular constituents

3   such as axons, which change dynamically over the course of subplate development.

4   In this study, we incorporate dynamically-evolving fiber (axon) populations into simulations of brain folding, such

5   that viscoelastic growth of the subplate depends on both the orientation and density of fibers in the tissue.

6   Importantly, growth only occurs in fiber populations, such that an axially stretched axon may grow along its length

7   but not in directions perpendicular to this axis. As a consequence, the dominant fiber orientation at a given location

8   within the subplate evolves based on the cumulative forces it has experienced. Simulations predict the development

9   of distinct patterns of fiber orientations beneath gyri and sulci, which emerge as a consequence of folding-induced

10   stresses. In order to determine whether such patterns can be found in developing brain tissue, high resolution *ex vivo*

11   diffusion tensor imaging (DTI) was performed on fetal rhesus macaque brains at developmental stages in which gyri

12   and sulci are forming, gestational ages (G)85 and G110. Water diffusion in the subplate proximal to the cortical

13   plate is indeed found to exhibit anisotropy, with the least restriction direction of displacement parallel to the primary

14   fiber orientation predicted by simulations. Together, these results support a novel paradigm in which cortical folding

15   influences subcortical organization, rather than only vice versa. This demonstration that mechanical stresses are

16   sufficient to induce realistic fiber orientation distributions provides further evidence for cortical expansion-induced

17   folding, as well as a new role of tension-induced axon growth in neuronal development that is of relevance to the

18   interpretation of abnormal folding patterns observed in mature brains.
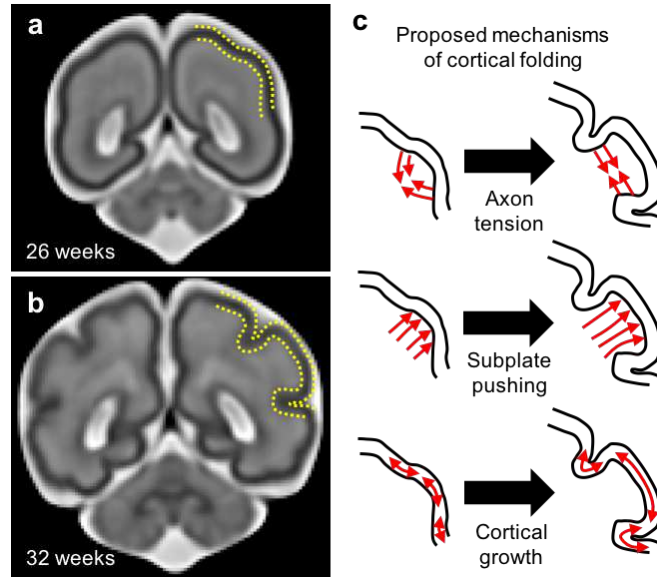
Figure 1. Cortical folding and subcortical organization. (a-b) *Magnetic resonance images of the fetal human brain at the onset of cortical folding (a) and after formation of cortical folds (b). Magnetic resonance images of the fetal human brain taken from Gholipour et al[19]. (c) Mechanisms proposed to actively induce cortical folding include axon tension that pulls together specific areas of cortex (top), subplate growth that exerts an outward push to form gyri (middle), and constrained cortical growth that induces mechanical buckling or creasing (bottom).*

2. Results

2.1. Subcortical growth based on mechanical feedback predicts asymptotic increase in fiber density.

To model subplate reorganization based on mechanical feedback, new constitutive equations were required to describe the biological behavior of viscoelastic fibers (axons and other processes such as radial glial scaffolds) embedded in a soft tissue (cell bodies, extracellular matrix, water).

In continuum mechanics, observable deformation of biological tissue can be conceptualized as a combination of growth, the deformation due to increases in size or number of cells and cell processes, and elastic deformation, the deformation due to mechanical tension or compression[20]. The total observable deformation is described mathematically by the three-dimensional tensor

1
$$\mathbf{F} = \mathbf{F}^* \cdot \mathbf{G} \tag{1}$$

2 where $\mathbf{F}^*$ is the elastic deformation tensor and $\mathbf{G}$ is the growth tensor. In the cortex, growth can be simply defined to

3 occur at constant rate (see *Materials and Methods*), as a consequence of biological processes including the

4 intercalation of cells into the cortex[21] and tangential expansion of cortical neuropil[22]. In subcortical layers, however,

5 viscoelastic fibers must be defined to grow or shrink in response to mechanical tension or compression, respectively.

6 This response has been studied extensively in axons from a variety of adult and embryonic sources[14-16,23], and more

7 recently in fibers of non-neuronal cells such as astrocytes[24]. Importantly, growing fibers represent just one

8 component of the total subplate tissue. Thus, at each time point, the overall tissue growth rate in each orthogonal

9 direction (*i*) is defined as

10
$$\frac{\partial G_i}{\partial t} = f_i a(\sigma_i - \sigma_0)G_i \tag{2}$$

11 where G_i is the total growth in direction i, f_i is the volume fraction of fibers oriented parallel to direction i, σ_i is the

12 mechanical stress experienced by the tissue in direction i, and a is stress-dependent growth rate. The target stress

13 (the threshold above which stress-dependent growth occurs), σ_0, was set at zero, consistent with experimental studies

14 suggesting an extremely low threshold for tension-based neurite elongation in embryonic forebrain neurons[23,25,26] as

15 well as previous models[10,17].

16 Based on histological studies suggesting that axonal fibers of the subplate are sparse and disorganized prior to

17 folding[7], fiber volume fractions were defined to be uniformly distributed and account for only a small fraction of the

18 overall tissue volume at the outset of all simulations. However, as the model progresses, Eq (2) dictates that only

19 fiber components of subcortical tissue grow in response to stress, with fibers only permitted to grow in the direction

20 of applied tension. Based on these assumptions, the fiber volume fractions evolve over time according to the

21 function

22
$$f_i(t) = \frac{V_{fibers,i}}{V_{total}} = \frac{G_i(t)f_{i,0}}{\sum_{j=1}^{3} G_j(t)f_{j,0} + f_{c,0}} \tag{3}$$

23 where $f_{i,0}$ is the initial volume fraction of fibers in direction i, and $f_{c,0}$ is the initial volume fraction of non-fiber

24 components (cells, extracellular matrix, and water), which do not grow.
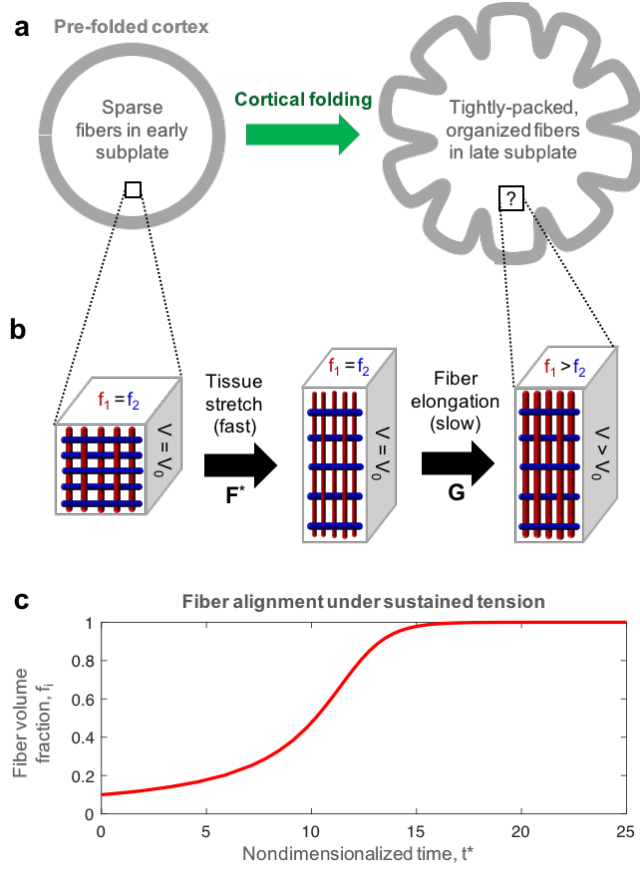
Figure 2. Tissue remodeling based on mechanical feedback. *(a) Expected subplate changes reported over the period of folding. (b) Hypothetical tissue volume element with embedded fibers in initial configuration (left), immediately after stretch (middle), and after fiber growth to relieve tension over a short period of time (right). V_0=initial volume, V=current volume, f_i=volume fraction of fibers in i-direction. (c) Theoretical solution for sustained uniaxial tension ($\sigma_{i,0}$) over time (nondimensionalized such that $t^*=a\sigma_{i,0}t$), starting from an initial fiber volume fraction of 10%.*

The physical consequences of these assumptions are illustrated in Fig. 2. For a block of tissue subjected to uniaxial tension, fibers parallel to the direction of applied tension will slowly elongate ($G_i>1$), leading to an increase in the total volume of fibers aligned in this direction. Due to Poisson's effect, compressive stresses perpendicular to the applied tension may also cause perpendicular fibers to shrink slightly. As a result of these effects, the volume fraction of fibers parallel to the applied tension (f_i) increases, with f_i slowly approaching 1 as time approaches

1 infinity (Fig. 2c). This behavior is predicted for all cases in which $a>0$, with a controlling the rate at which fiber

2 growth and remodeling occurs under sustained stress, $\sigma_{i,0}$. At the global level, an increase in fiber volume fraction is

3 consistent with reported increases in subcortical fiber content over the course of cortical folding[7], during which

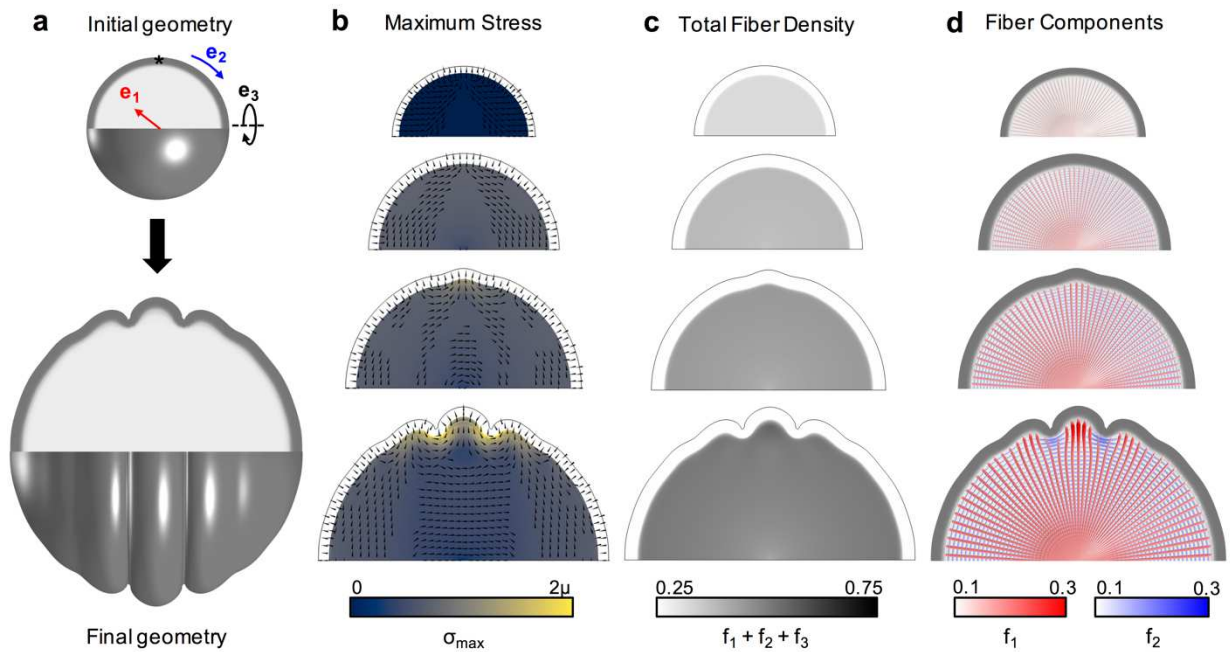4 subcortical layers are generally held in a state of tension[10].

1 **2.2. Cortical folding stresses induce stereotyped pattern in developing fiber networks**.

2 To characterize the influence of mechanical feedback on fiber organization in the subplate (Fig. 1), the growth

3 behavior described in Eqs 1-3 was applied to a simple three-dimensional model of cortical folding. First, we

4 considered a spherical initial geometry to approximate the curved shape of the unfolded brain (Fig. 3a). This

5 symmetric geometry avoids folding biases induced by curvature variations[11,13] and enables precise control over other

6 factors that may bias the initial direction of folding[11,17,18]. To break symmetry and induce the first fold, a small

7 region of the cortex was defined to grow 5% faster than adjacent cortex, consistent with measured variations that

8 have been proposed to influence formation of primary folds[27]. Cortical growth rate was set at $g_c=0.02$ days^{-1} (d^{-1}),

9 based on total surface area change observed during early rhesus macaque development[28], such that the total

10 simulation time spans a period of 50 gestational days and a 6-fold increase in cortical surface area.

11 Material radial, circumferential, and meridional orientations were defined from the initial spherical coordinate

12 system (e_1, e_2, e_3, respectively) and tracked over the course of deformation. In gyrencephalic species, radial glial

13 fibers have been reported within the subplate prior to folding, in addition to more randomly-oriented axonal fibers[29].

14 To match the weak radial orientation observed in early subcortical layers, initial radial and tangential fiber volume

15 fractions were defined as $f_{1,0}=0.12$ and $f_{2,0}=f_{3,0}=0.1$, respectively. To determine a reasonable range of values for the

16 stress-dependent fiber growth parameter, a, we examined prior neurite elongation experiments, which are diverse in

17 terms of neuron type, magnitude of applied stretch or stress, and parameters measured (Supplementary Table 1). For

18 studies reporting force-dependent elongation rates, calculated values of a ranged from 0.02 Pa^{-1}d^{-1} in chick

19 embryonic forebrain neurons[25,26] to 0.1 Pa^{-1}d^{-1} in chick embryonic dorsal root ganglia neurons[30]. For experiments

20 reporting stretch-dependent elongation rates[18,31], conversion based on reported Young's modulus for individual

21 neurites, ranging 100-4,600 Pa[32,33] yields the range $a = 0.0004$-0.02 Pa^{-1}d^{-1}. Recent experiments using ultra-long

22 astrocyte processes, designed to mimic radial glial scaffolds, have also reported viscoelastic behavior, though

stretch-dependent elongation rates were four to six times slower than rates in neurites[24]. The following simulation

2 results considered a value of approximately $a = 0.001$ Pa^{-1}d^{-1} for all fibers, though model behavior across the full

3 range of values was also explored (Supplementary Figure 1).

4 Fig. 3 depicts the progression subplate organization over the period of cortical expansion and folding, with

5 nondimensionalized simulation time, $T = g_c t$, ranging from 0 to 1. Prior to cortical folding, cortical expansion

6 induced low levels of tension throughout the subplate (Fig. 3b). As folding commenced, tension that evolved

7 beneath prospective sulci was primarily tangential, while tension that evolved beneath prospective gyri was

8 primarily radial, consistent with mechanical stresses measured in the developing ferret[10]. As a consequence of fiber

9 elongation in response to stress, tension throughout the subplate caused total fiber volume fraction to increase

10 steadily over time (Fig. 3c). Furthermore, localized patterns of stress led to increased tangential fiber volume

11 fraction and decreased radial fiber volume fraction beneath sulci (Fig. 3d). Similarly, increased radial tension

12 beneath gyri led to increased radial fiber volume fraction.

13

15 ***Figure 3. Cortical folding induces stereotyped fiber organization beneath gyri and sulci. (a)*** *Model geometry*

16 *before and after folding. For the axisymmetric model, material coordinate directions are defined in radial (**e₁**),*

17 *circumferential-tangential (**e₂**), and axisymmetric-tangential directions (**e₃**), and can be followed over the course of*
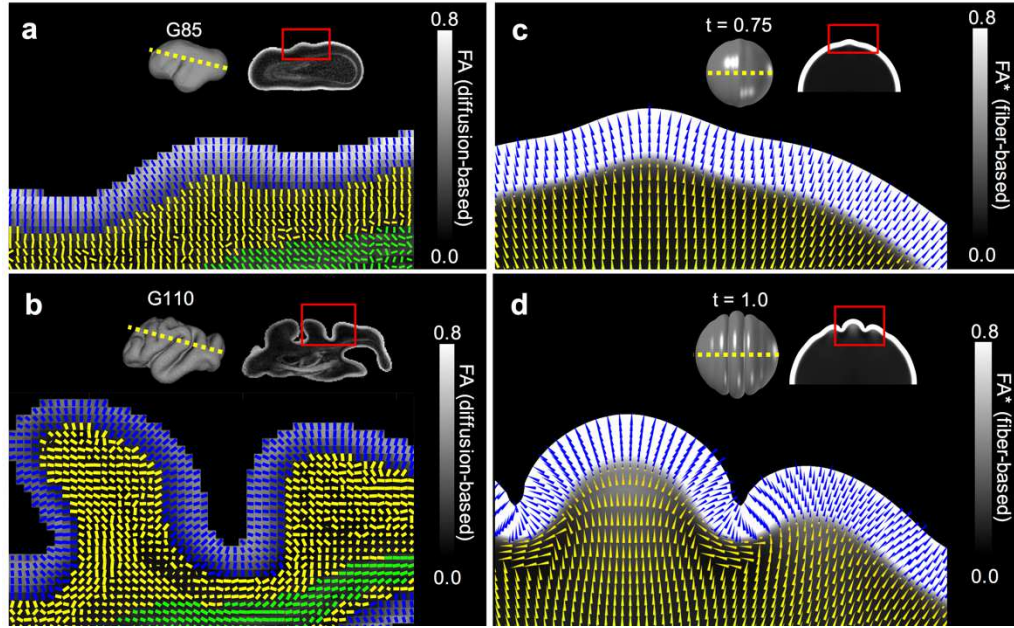
*deformation. Asterisk denotes location of symmetry-breaking perturbation. **(b-d)** Evolution of maximum*

nondimensionalized Cauchy stress (tension), total fiber density, and directional fiber components in the subplate

over the course of folding (from top to bottom, simulation time T=0, 0.5, 0.75, 1). In (d), fiber volume fraction in a

given direction is represented by both color and line thickness.

2.3. Experimental evidence supports the predicted pattern of fiber orientations within the subplate.

To validate subplate anisotropy predicted in simulations, high resolution DTI measurements were performed on *ex vivo* fetal rhesus macaque brains. In these results, the primary eigenvector of the diffusion tensor is expected to be colinear with the dominant fiber orientation within a given image voxel. Primary eigenvectors for data collected from a gestational day (G)85 and G110, of a 168 day gestational term for rhesus macaques, are shown in Fig. 4a and 4b, respectively.

Fig. 4a (inset) shows a lateral view of the G85 cerebral cortical surface, and a fractional anisotropy (FA) parameter map of a slice oriented as indicated with the yellow dashed line. This gestational age is when folding of the cerebral cortex is first initiated, and only rudimentary grooves, which will mature into the superior temporal sulcus and sylvian fissure, are observable. As documented previously, FA within the cortical plate at this gestational age was uniformly high (approximately 0.7-0.8)[28,29]. In contrast, FA within the subplate is extremely low (0.1-0.2)[29]. Fig. 4a (main) shows primary eigenvector maps within the area indicated by the red rectangle of the inset image. Primary eigenvector directions are shown for the cortical plate (blue lines), subplate (yellow lines), and deeper layers (green lines) including the outer fibrous layer, outer subventricular zone, inner fibrous layer, inner subventricular zone and ventricular zone. In spite of the low FA value, the primary eigenvector orientation is radially oriented within the subplate, which may be attributed to the influence of radial glial fibers. No evidence of tangential subplate organization was observed beneath early-stage sulci, contradicting prior interpretations that subplate orientation drives formation of folds[8,18]. However, this observation is consistent with our model (Fig. 4c) in which the primary eigenvector direction, calculated from fiber volume fractions, remained slightly radial from model initiation (initial fiber volume fractions set such that $f_{1,0} > f_{2,0} = f_{3,0}$) through early folding ($T = 0.75$).
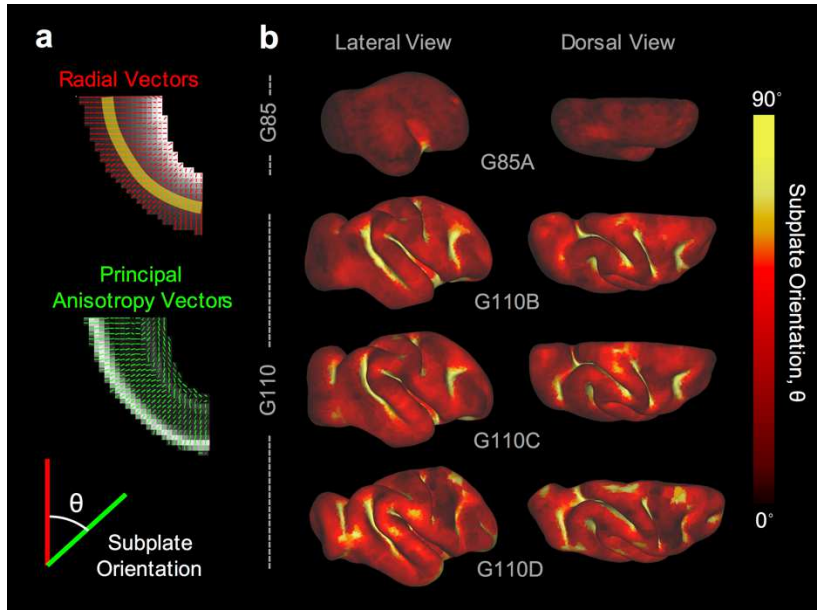
10

Fig. 4b shows the analogous FA map for a rhesus macaque at G110, after primary sulci have formed. Although the

magnitude of FA within the subplate remains much lower than within the cortical plate, the orientations of primary

eigenvectors within the subplate neighboring the sulcus have changed from a radial to a tangential orientation. The

tangential orientation of primary eigenvectors within the subplate beneath the sulci is consistent with the tangential

orientation found beneath sulci in our model (Fig. 4d).

Figure 4. Anisotropy in the developing subplate matches model predictions. (a-b) *Primary eigenvector directions*

(tick marks) based on high-resolution DTI of the rhesus macaque brain at G85 (a) and G110 (b), at the slice

indicated by the yellow dotted line and location indicated by the red box. Fractional anisotropy (FA) maps are

shown as an underlay. ***(c-d)*** *Primary eigenvector directions (tick marks) based on the fiber volume fractions*

predicted by our model at the onset of folding (c) and after fold formation (d). FA* maps are based on the 3D tensor

describing model subplate volume fractions, with cortical FA* (not defined in model) set to 1 for visualization. Tick

marks are colored such that blue=cortex, yellow=subplate, green=deeper subcortical layers.

The primary eigenvector maps of Fig. 4 suggest consistency between primary eigenvector orientations measured

with diffusion (reflecting fiber orientation) and primary eigenvector orientations calculated directly from simulated

fiber volume fractions. However, only a small brain region is shown, representing a projection of 3D information

1   onto a 2D plane. In order to confirm that the observed orientations are consistent with respect to gyri and sulci

2   throughout the rhesus macaque brain, and that the tangential orientation observed near sulcal fundi are observable

3   irrespective of projection plane orientation, angles between primary diffusion tensor eigenvectors and the local

4   radial directions were calculated throughout the entire brain for four developing subjects. Primary eigenvector

5   angles in the superficial subplate were quantified as shown in Fig. 5, with 0 degrees indicating radial alignment and

6   90 degrees indicating tangential alignment (parallel to the cortical surface).

7

8   *Figure 5. Primary anisotropy orientation across subplate in developing rhesus macaque. (a) Radial orientation*

9   *vectors generated from a gradient representing distance from the cortical surface (red), and primary eigenvectors*

10   *generated from DTI (green). For voxels at a set distance from the cortical surface (illustrated by yellow strip),*

11   *subplate orientation angle was calculated as the angle between the radial (red) and principal anisotropy (green)*

12   *vectors. (b) Subplate orientation angle mapped onto cortical surface reconstructions for one G85 (top) and three*

13   *individual G110 (bottom) brains. Panel (a) modified from Wang et al[29].*

14

15   For all sulci, primary eigenvectors of the subjacent subplate were oriented in a tangential direction. In addition, the

16   subplate beneath crowns of each gyrus consisted of primary eigenvectors with radial orientations. Results indicate

1   that tangential alignment near sulci, and radial alignment near gyri, is a general feature observed within the G110

2   brain, whereas no tangential alignment is observed prior to sulcification in the G85 subplate.

3

4   **2.4. Mechanical feedback may induce organization of deep fiber tracts**

5   Based on the effect of folding-induced stresses on subplate organization, we hypothesized that other mechanical

6   stresses may induce additional features subcortical fiber organization. To test this hypothesis, alternative model

7   geometries were considered to more closely approximate structural features of the developing brain.
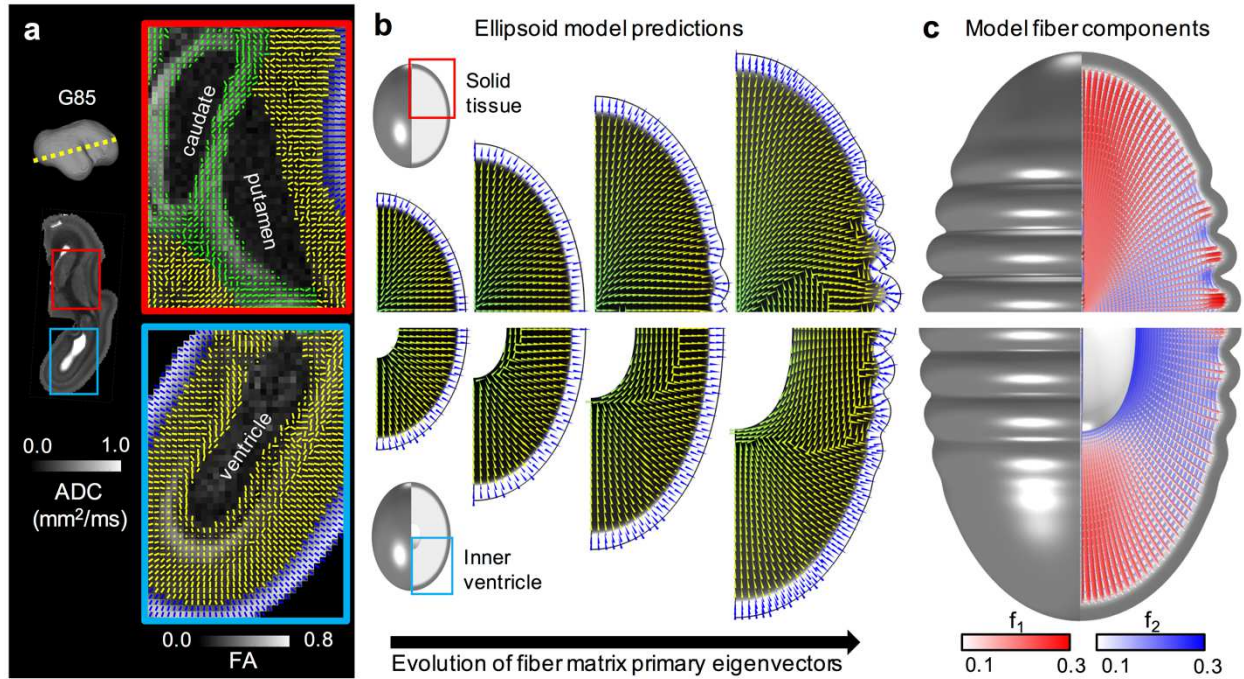
8   To approximate the elongated structure of the temporal lobe or an entire hemisphere (anterior-posterior axis longer

9   than superior-inferior or medial-lateral), an ellipsoidal – rather than spherical – initial shape was selected. Since the

10   curvature variation in an ellipsoid is sufficient to bias the location of the first fold, no variation in cortical growth

11   was necessary to break symmetry in these simulations. To examine the effect of deep brain structures, two models

12   were considered: (i) an ellipsoid containing solid tissue, to approximate deep gray matter structures, and (ii) an

13   ellipsoid containing a tissue-less inner lumen, to approximate a cerebrospinal fluid-filled lateral ventricle. Fig. 6

14   depicts the progression of subplate organization for each case.

15   In contrast to spherical models (Fig. 3), both ellipsoidal models predicted increased tension along the length of

16   ellipsoid, resulting in more tangentially-organized fibers in the middle of the ellipsoid and more radially-organized

17   fibers at the poles (Fig. 6c). In models with an inner ventricle, cortical expansion also predicted strong tangential

18   tension near the ventricular surface, leading to a primarily tangential orientation along the ventricle. For the

19   ellipsoidal case shown (Fig. 6, bottom), tangential organization was first apparent along the middle third of the

20   ventricle but eventually propagated to the poles as well. These trends are consistent with high tensile forces near the

21   ventricle in the developing ferret brain[10] and anisotropy previously reported in the rhesus macaque prior to folding[29].

22   By contrast, models with a solid inner core generally maintained radial organization throughout deeper layers (Fig.

23   3), with the exception of a relatively weak tangential organization along the middle of ellipsoidal models (Fig. 6,

24   top).

25   To confirm these predictions, model fiber orientations were again compared to high resolution DTI in the rhesus

26   macaque. As shown in Fig. 6a (bottom), FA increased and tangential primary eigenvectors were visible near the

1 ventricle in the G85 macaque brain, consistent with previous reports by Wang and colleagues[29] (Fig. 5a).

2 Furthermore, tangential organization along the ventricle was most apparent in the lower curvature portion (along its

3 length), suggesting that organization near the poles occurs later, consistent with the predicted time course of the

4 ellipsoidal model with ventricle (Fig. 6b-c, bottom). By contrast, low FA and radial organization persisted above

5 solid deep-brain structures such as the basal ganglia (Fig. 6a, top).

6

7

8 *Figure 6. Stresses predict accurate trends with respect to deep fiber tracts. (a) Primary eigenvector directions (tick*

9 *marks) based on high-resolution DTI of the rhesus macaque brain at G85 at the slice indicated by the yellow dotted*

10 *line and locations indicated by the red and blue boxes (ADC map shown to visualize deep gray matter structures).*

11 *For maps showing primary eigenvector directions, fractional anisotropy (FA) maps are shown as an underlay.*

12 *Tangential orientation is visible along the ventricle prior to folding. (b) Primary eigenvector directions (tick marks)*

13 *based on the fiber volume fractions predicted by ellipsoidal models with solid core of tissue (top) and open inner*

14 *ventricle (bottom). (From left to right, T=0, 0.5, 0.75, 1.) FA* underlay is based on the 3D tensor describing volume*

15 *fractions in our model (see Materials and Methods for details). Tick marks are colored such that blue=cortex,*

16 *yellow=subplate, green=deep brain structures. (c) Directional fiber components at T=1, with fiber volume fraction*

1   *in a given direction represented by both color and line thickness. On an ellipsoidal geometry, tangential fibers*

2   *accumulate first and in greater magnitude along the longer axis, both along the ventricle and in intermediate layers.*

3

4 **<u>3. Discussion</u>**

5 Stretch-induced elongation of axons has been well established in cultured neurons[14,16,23,31], and previous models

6 have proposed a role for this phenomenon in gyrencephalic brain development[17]. However, to date, mechanics-based

7 investigations have struggled to reconcile the mechanical features of developing brain tissue[10] with the

8 organizational features hypothesized to influence brain morphology. In this work, we extend previous strategies for

9 simulating brain folding by incorporating subplate remodeling via stress-induced growth of fiber populations. The

10 resulting mechanobiological model facilitates predictions of not only cortical morphology, but also primary fiber

11 orientations observed in the developing subplate. Starting from a smooth cortex and unpatterned subplate,

12 simulations predict consistent patterns in subplate fiber organization as the result of cortical expansion and folding.

13 Predicted spatial and temporal relationships are supported by DTI measurements of fiber orientations in the

14 developing rhesus brain, as well as previously reported mechanical measures. Mechanobiologically-induced patterns

15 described in this study may relate to features of normal and abnormal white matter organization observed across

16 gyrencephalic species including human.

17 **Linking microscopic measures of viscoelasticity to macroscopic models of folding.**

18 In this study, we defined and tracked growing fibers as a specific tissue component within the subplate. This

19 approach offers significant advantages over previous models, which considered the subplate as either a homogenous

20 composite material[10,17] or an anisotropic but static matrix of fibers[18]. First, this approach enables simulation of

21 subplate tissue remodeling, with the goal of recapitulating the dramatic change in subcortical fiber content observed

22 during the period of folding[7-9]. As illustrated in both the simple solution for uniaxial stretch (Fig. 2) and the 3D

23 finite-element simulation of cortical expansion and folding (Fig. 3), a state of sustained subplate tension predicts

24 increasing fiber content, consistent with observations during development[7]. Second, this approach enables more

25 precise application of viscoelastic properties reported in previous studies, such as individual axon elongation

26 experiments.

1   Review of the previous elongation experiments revealed considerable variability in experimental approaches and

2   reported viscoelastic parameters (Supplementary Table 1), highlighting the need for accurate and consistent physical

3   measures. Furthermore, even among methodologically similar studies, a wide range of axon elongation rates were

4   observed for different neuron types, at different stages of maturation. These differences may relate to availability of

5   biological resources such as cytoskeletal proteins required to elongate neurites, which may be developmentally

6   regulated[34]. Fewer experimental studies have considered the viscoelastic behavior of non-neural tissue components.

7   However, radial glial leading edges have been shown to extend at rates comparable to axonal growth cones[35], and

8   astrocyte processes have been shown to elongate under sustained tension in vitro, though at a slower rate[24].

9   Additional studies are needed to clarify the rates of tension-induced elongation of various fiber types in the context

10   of brain folding, ideally in relevant gyrencephalic model systems such as the developing ferret or rhesus macaque.

11   In this study, we showed that a model using realistic parameter values, based on axon elongation studies and other

12   experimentally-measured properties, can reproduce normal folding morphologies. However, only fiber elongation

13   rates at the lower end of reported values produced a folded cortex (Supplementary Figure 1). By contrast, with

14   sufficiently fast fiber elongation, growth of the subplate kept pace with the expanding cortex, dissipating the

15   compressive stresses required to induce mechanical buckling or creasing. Past models have required even slower

16   viscoelastic rates to induce folding under similar geometric and boundary conditions[17,18]. The ability of our model to

17   induce folding under a broader range of viscoelastic growth rates can be attributed to the implementation of fiber

18   volume fractions, which results in a slower net growth of the subplate compared to models for which viscoelasticity

19   is uniformly applied. While simulations presented here do not distinguish fiber contributions from neuronal and non-

20   neuronal sources (neurites versus radial glial scaffolds), the need for values on the lower end of the experimentally-

21   reported range may reflect an early predominance of slower-growing fibers such as radial glial scaffolds[24].

22   Alternately, results may suggest a slower response of neurites under specific *in vivo* conditions during the period of

23   folding compared to *in vitro* experimental conditions.

24   Notably, previous studies have suggested a relationship between the rate of viscoelastic subplate response and

25   abnormal fold morphologies. Bayly and colleagues[17] showed that faster subplate response relative to cortical growth

26   can lead to decreased folding (lissencephaly or pachygyria), while slower subplate response can lead to many small

27   folds (polymicrogyria). By considering stress-dependent subplate fiber growth, additional insights may be gleaned in

1 terms of white matter organization. For example, both lissencephaly and polymicrogyria have been associated with

2 reduced short-range association fibers in human[36,37]. In our framework, slower fiber elongation predicts not only

3 increased gyrification (polymicrogyria) but also reduced overall fiber density (Supplemental Fig. 1a), consistent

4 with reduced short and long-range connections reported in polymicrogyria[37]. Conversely, faster fiber elongation

5 relative to cortical expansion predicts reduced gyrification but high overall fiber density. Consistent with

6 observations in lissencephaly, simulations with fast fiber elongation predict the absence of folds leads to a reduction

7 of tangentially-oriented fibers beneath sulci (short-range cortico-cortical pathways) but preservation of radially-

8 oriented fibers (projection pathways) (Supplemental Fig. 1b)[36].

9 **Axon organization as a consequence, rather than a cause, of cortical morphogenesis**

10 In contrast to previous hypotheses that subcortical organization drives patterns cortical folding (Fig. 1), this study

11 proposes a novel a framework in which folding-induced tension drives patterns of axon organization beneath gyri

12 and sulci (Fig. 3). Two lines of experimental evidence support this generalizable relationship in developing

13 gyrencephalic brains.

14 First, the pattern of subplate tension predicted by our model – which is greatest along tangential directions subjacent

15 to sulci, but radial subjacent to gyri – is consistent with the directions of tension measured in developing ferret brain

16 tissue slices[10]. Previous models of cortical expansion-driven folding, including those without viscoelastic or fiber

17 components, have also predicted subcortical stresses consistent with these measures[10,38,11,17,18], but failed to link

18 these patterns to developing subplate organization. By contrast, competing hypotheses for folding (Fig. 1) have

19 focused on this observed link, but predict tension patterns inconsistent with tension measurements[22]. For example, if

20 axon-induced tension "pulled" two regions of cortical plate together to form the walls of a gyrus or tether sulci

21 down[6] (Fig. 1, top), tension would be higher tangentially subjacent to gyri and radially subjacent to sulci.

22 Alternately, if the subplate exerted outward force on regions of the cortical plate destined to become gyral crowns[7-9]

23 (Fig. 1, middle), radial compression, rather than the observed tension, would be expected subjacent to gyri.

24 Second, in this study we showed that DTI data from *ex vivo* fetal rhesus brain tissue exhibits a highly consistent

25 pattern across all gyri and sulci at the gestational age in which cortical folds have recently formed (G110, Figs. 4-5).

26 Within subplate tissue, the primary eigenvector of the diffusion tensor is parallel to the tangent plane of the pial

surface beneath sulci, while primary eigenvectors are radially-oriented in subplate beneath gyral crowns. Thus, the DTI data supports the model predictions that (i) tangentially-oriented subplate fibers are more abundant (i.e. have a higher volume fraction) than radially-oriented fibers at the base of sulci and (ii) radially-oriented subplate fibers are more abundant in the crowns of gyri. By contrast, results are inconsistent with the hypothesis that axons pull the cortex to form gyri, which would predict a reversed pattern of predominant axon orientations[6]. Model predictions in this study are also consistent with tractography studies using fetal human DTI, in which Takahashi and colleagues[8] reported fibers sweeping tangentially beneath sulci and radially into gyral crowns, similar to U-shaped short association fibers observed in the adult brain. However, contrary to interpretations suggesting subplate heterogeneity precedes and influences cortical folds[7-9], our study found no evidence of tangential subplate orientation prior to folding, even once early sulci could be clearly delineated (G85, Figs. 4). Previous simulations of cortical expansion-induced folding have illustrated the potential for pre-existing subplate orientations to bias the location and direction of folds[18]. While the results of this study do not rule out the potential influence of early subplate organization, simulations illustrate that pre-existing patterns are not required to produce the observed link between folding and subplate organization.

Finally, based on the evidence supporting a relationship between folding-induced stresses and subplate organization, we considered the possibility that other mechanical stresses could contribute to white matter organization. Notably, in ellipsoidal models, we observed increased tension parallel to the long axis, prior to the onset of folding. The resulting accumulation of longitudinal fibers is strikingly similar to deep longitudinal fasiculi that span the long axis of the human brain: the superior longitudinal fasiculus, which runs from the frontal to occipital lobe, and the inferior longitudinal fasiculus, which follows the length of the temporal lobe. Furthermore, models with an internal lumen predicted tangential fiber accumulation at the interface between tissue and cerebrospinal fluid, with earlier accumulation along the middle of an ellipsoid than at the poles. DTI of the G85 macaque confirmed similar tangential organization at early stages in the intermediate zone between the occipital and parietal lobes, but not at the occipital pole (Fig. 6A)[29]. Eventual organization along the full perimeter of the ventricle has been reported in slightly later stages of development[39,40]. This organization of fibers around the ventricle, which occurred prior to folding, is consistent with well-established axon tracts, such as the corpus callosum and optic radiations, that wrap around the lateral ventricles in both gyrencephalic and lissencephalic species. By contrast, in models without a ventricle (Fig. 3 and Fig. 6 top), deep tangential tension did not develop and fiber orientation remained generally

1   radial. Just as tangential organization near the ventricle is consistent with tracts observed near the ventricular

2   surface, radial organization extending from solid structures may relate to projection fibers (eg., corona radiata) that

3   extend from deep structures such as the striatum. Therefore, we consider it possible that mechanical factors

4   contribute to the development of these early-developing axonal fiber populations.

5

6   **Implications for interpreting abnormal patterns of cortical folding**

7   Previously, cortical folding abnormalities associated with neurodevelopmental disorders have been interpreted from

8   the perspective that axon tension induces the formation of gyri and sulci. In this context, developmental mechanisms

9   that influence white matter development, such as axon guidance, have been implicated as contributing to disease

10   pathophysiology. However, here we present a role for mechanobiological cues, resulting from expansion and folding

11   of the cortical plate, to induce growth and organization of axons. Thus, future research may consider the possibility

12   that the neurodevelopmental disorder originates from disruptions to processes involved in expansion of the cortical

13   plate, such as morphological maturation of neurons and synaptogenesis.

14

15   **4. Methods**

16   **4.1. Mathematical Model and Simulation.**

17   All finite element simulations were performed using COMSOL Multiphysics software (version 5.3a, COMSOL Inc.,

18   Burlington, MA). Both spherical and ellipsoidal models utilized an axisymmetric domain and assumed quasi-static,

19   time-dependent solutions. As in previous models of brain folding[10,38], the elastic response of developing brain tissue

20   ($\mathbf{F}^*$) was modeled as a standard neo-Hookean material:

21
$$W = \frac{\mu}{2}\left(J^{*-\frac{2}{3}}tr(\mathbf{F}^{*\mathrm{T}} \cdot \mathbf{F}^*) - 3\right) + \frac{\kappa}{2}(J^* - 1)^2. \tag{4}$$

22   Here we considered a shear modulus μ=300 Pa and bulk modulus κ=100μ, based on material properties derived from

23   previous studies[10,17,41]. The three-dimensional (3D) growth tensor, $\mathbf{G}$, was defined to include orthogonal growth

24   components such that

1              $$G = G_1\mathbf{e_1}\mathbf{e_1} + G_2\mathbf{e_2}\mathbf{e_2} + G_3\mathbf{e_3}\mathbf{e_3}.$$ (5)

2   To simulate cortical surface area expansion, growth rate was defined in the cortex such that

3             $$\frac{\partial G_1}{\partial t} = 0, \frac{\partial G_2}{\partial t} = g_c G_2(t), \frac{\partial G_3}{\partial t} = g_c G_3(t).$$ (6)

4   These equations correspond to exponential growth in both tangential directions ($G_2 = G_3 = e^{g_c t}$) and no growth in

5   the radial direction ($G_1 = 1$). Cortical growth rate, g_c, was estimated from an exponential fit of total surface area

6   change observed during early rhesus macaque development[28].

7   As described in Eq. 2, growth of subcortical layers was defined by stress-induced fiber elongation, where σ_i (i = 1 to

8   3) represent the radial, circumferential, and meridional components of the 3D Cauchy stress tensor, $\boldsymbol{\sigma}$. This stress

9   tensor is defined from the elastic deformation component of the total deformation tensor as

10             $$\sigma = J^{*-1}\mathbf{F}^* \cdot \frac{\partial W}{\partial \mathbf{F}^{*\mathrm{T}}},$$ (7)

11   where W is the strain energy density function and $J^* = \det(\mathbf{F}^*)$, the ratio of volume change due to elastic

12   deformation.

13   A range of values was considered for the stress-dependent fiber growth parameter, a, based on reported measures

14   from previous studies, as described in Supplementary Table 1. For studies that reported force-dependent elongation

15   rate (b, change in length per unit force per unit time), a was directly calculated as $a=bA/L$, where L represents initial

16   neurite length and A represents neurite cross-sectional area. For studies that reported stretch-dependent elongation

17   rate (G^{axon}), a was approximated by assuming the stress-strain relationship for uniaxial stress and small deformations

18   ($\sigma=E\varepsilon$), such that $a = G^{\mathrm{axon}}/E$. Main results in this paper considered a value of approximately $a = 0.001$ Pa^{-1}d^{-1}, with

19   the effects of other possible values explored in *Supplemental Information*.

20   **4.2. Magnetic Resonance Imaging and Analysis**.

21   Ex vivo MRI scans were performed on four rhesus monkey brains, one form a control fetus perfusion fixed at G85,

22   and three from three other control fetuses perfusion fixed at G110[42]. Postmortem fetal brains were cut into

23   hemispheres and the right hemispheres were immersed in Fluorinert Electronic Liquid FC-77 (3M, St. Paul, MN)

1 during MRI scans and returned to PBS immediately afterwards. Experiments were performed on an 11.7 T small-

2 animal MRI system (Bruker, Rheinstetten, Germany) and a custom Helmholtz coil (5 cm diameter, 5 cm length) was

3 used for radiofrequency transmission and reception. A multi-slice spin-echo pulse sequence (TR/TE = 15 s/30 ms),

4 incorporating a Stejskal–Tanner diffusion sensitization gradient pair was used to acquire diffusion MRI data at an

5 isotropic resolution of 0.3 mm for G110 hemispheres and 0.2 mm for the G85 hemisphere. A 25-direction,

6 icosahedral sampling scheme[43] was utilized for all experiments with 3 b0 images, and diffusion weighted images

7 with a b-value of 2500 s/mm^2. Standard procedures were followed to calculate eigenvalues (λ_1, λ_2, and λ_3, listed

8 from smallest to largest) and eigenvectors (v_1, v_2, and v_3). DTI indices such as FA and ADC were calculated from

9 the eigenvalues for each voxel.

10 Brain segmentation was achieved by first intensity thresholding and then manual editing on the ADC maps using

11 ITK-SNAP (http://www.itksnap.org [44]). The resulting segmentations were used as input for the "SureFit" operation

12 in the CARET software package (http://brainvis.wustl.edu [45]) to generate cortical pial surface representations.

13 To determine the dominant fiber orientation relative to the local radial direction (e_1) of a given voxel, θ, the angle

14 between v_1 and the cortical surface norm, were estimated as illustrated in Fig. 5a. First, a distance matrix from pial

15 surface was computed for each voxel from the whole brain segmentation. Then, a 3D gradient of the distance matrix

16 was derived and, for a given voxel, oriented along the radial direction. θ, with the unit of degree and range of $0 - 90$,

17 was calculated for each voxel. A small θ indicates v_1 is more radially aligned whereas a large θ indicated v_1 is more

18 tangentially aligned relative to cortical surface. To visualize θ within the superficial subplate across gyri and sulci,

19 the superficial subplate (layer 4 in [29]) were manually segmented and θ within this region were averaged from a

20 radius of 2 voxels and projected to the nearest cortical nodes.

21 **5.3. Primary Fiber Orientation and Fractional Anisotropy Comparisons.**

22 For MRI data obtained in the rhesus macaque, primary eigenvectors and fractional anisotropy (FA) were calculated

23 from the DTI scatter matrix using standard definitions. While these diffusion-based values offer an indirect measure

24 of tissue properties, they are thought to generally reflect primary fiber orientations and tissue anisotropy resulting

25 primarily from fiber distributions, though other factors such as myelination and stress state of various tissue

26 components (permeability) also likely influence these maps. Thus, as a first approximation for simulation

1 comparisons, primary eigenvectors and fractional anisotropy were calculated from fiber and non-fiber tissue volume

2 fractions as described below.

3 First, a matrix describing the initial (orthogonal) fiber volume fractions was defined in the reference coordinate

4 frame as:

$$\mathbf{A} = \begin{bmatrix} f_1 & 0 & 0 \\ 0 & f_2 & 0 \\ 0 & 0 & f_3 \end{bmatrix} \tag{7}$$

6 The coordinate transformation $\mathbf{A'} = \mathbf{F}^{\mathrm{T}} \cdot \mathbf{A} \cdot \mathbf{F}$ was applied account for rotations from the reference (initial) to

7 deformed (final) configuration, which induces shear (non-orthogonal) components in the deformed configuration.

8 Principal eigenvectors and eigenvalues of $\mathbf{A'}$ ($\mathbf{v'_i}$ and λ'_i, respectively) were calculated using COMSOL built-in

9 functions. Similarly, the deformed radial direction was tracked with the coordinate transformation $\mathbf{u'_1} = \mathbf{F} \cdot \mathbf{u_1}$ to

10 allow calculation of angle θ between the radial direction, $\mathbf{u'_1}$, and first principal eigenvector, $\mathbf{v'_1}$.

11 Fractional anisotropy, which is 0 for a fully isotropic tissue and 1 for a maximally anisotropic tissue, incorporates

12 information from not only fiber volume fractions, but also the isotropic tissue components represented by f_c, which

13 is distributed equally among the three principal eigenvector directions. Thus, simulated fractional anisotropy, FA*,

14 was defined at each point as follows

$$FA^* = \sqrt{\frac{(\lambda_1^* - \lambda_2^*)^2 + (\lambda_2^* - \lambda_3^*)^2 + (\lambda_1^* - \lambda_3^*)^2}{2(\lambda_1^{*2} + \lambda_3^{*2} + \lambda_3^{*2})}} \tag{9}$$

16 where $\lambda_i^* = \lambda_i' + f_c/3$, to account for the volume fraction of isotropic tissue that is distributed equally among the

17 three principal eigenvector directions.

22

5. References

1   Ristić, A. J. *et al.* Cortical thickness, surface area and folding in patients with psychogenic nonepileptic seizures. *Epilepsy research* **112**, 84-91 (2015).

2   Nordahl, C. W. *et al.* Cortical folding abnormalities in autism revealed by surface-based morphometry. *Journal of Neuroscience* **27**, 11725-11735 (2007).

3   Penttilä, J. *et al.* Cortical folding in patients with bipolar disorder or unipolar depression. *Journal of Psychiatry & Neuroscience: JPN* **34**, 127 (2009).

4   Csernansky, J. G. *et al.* Symmetric abnormalities in sulcal patterning in schizophrenia. *Neuroimage* **43**, 440-446 (2008).

5   Rakic, P. Specification of cerebral cortical areas. *Science* **241**, 170-176 (1988).

6   Van Essen, D. C. A tension-based theory of morphogenesis and compact wiring in the central nervous system. *Nature* **385**, 313-318 (1997).

7   Kostovic, I. & Rakic, P. Developmental history of the transient subplate zone in the visual and somatosensory cortex of the macaque monkey and human brain. *Journal of Comparative Neurology* **297**, 441-470 (1990).

8   Takahashi, E., Folkerth, R. D., Galaburda, A. M. & Grant, P. E. Emerging cerebral connectivity in the human fetal brain: an MR tractography study. *Cerebral cortex* **22**, 455-464 (2012).

9   Rana, S. *et al.* The Subplate: A Potential Driver of Cortical Folding? **29**, 4697-4708 (2019).

10   Xu, G. *et al.* Axons pull on the brain, but tension does not drive cortical folding. *Journal of biomechanical engineering* **132**, 071013 (2010).

11   Richman, D. P., Stewart, R. M., Hutchinson, J. W. & Caviness, V. S. Mechanical model of brain convolutional development. *Science* **189**, 18-21 (1975).

12   Toro, R. & Burnod, Y. J. C. c. A morphogenetic model for the development of cortical convolutions. **15**, 1900-1913 (2005).

13   Tallinen, T. *et al.* On the growth and form of cortical convolutions. *Nature Physics* **12**, 588-593 (2016).

14   Bray, D. Axonal growth in response to experimentally applied mechanical tension. *Developmental biology* **102**, 379-389 (1984).

15   Dennerll, T. J., Lamoureux, P., Buxbaum, R. E. & Heidemann, S. R. The cytomechanics of axonal elongation and retraction. *The Journal of cell biology* **109**, 3073-3083 (1989).

16   Heidemann, S. R. & Buxbaum, R. E. Tension as a regulator and integrator of axonal growth. *Cell motility the cytoskeleton* **17**, 6-10 (1990).

17   Bayly, P., Okamoto, R., Xu, G., Shi, Y. & Taber, L. A cortical folding model incorporating stress-dependent growth explains gyral wavelengths and stress patterns in the developing brain. *Physical biology* **10**, 016005 (2013).

18   Holland, M. A., Miller, K. E. & Kuhl, E. Emerging brain morphologies from axonal elongation. *Annals of biomedical engineering* **43**, 1640-1653 (2015).

19   Gholipour, A. *et al.* A normative spatiotemporal MRI atlas of the fetal brain for automatic segmentation and analysis of early brain growth. *Scientific reports* **7**, 1-13 (2017).

20   Rodriguez, E. K., Hoger, A. & McCulloch, A. D. Stress-dependent finite growth in soft elastic tissues. *Journal of biomechanics* **27**, 455-467 (1994).

21   Striedter, G. F., Srinivasan, S. & Monuki, E. S. Cortical folding: when, where, how, and why? *Annual review of neuroscience* **38**, 291-307 (2015).

22   Garcia, K., Kroenke, C. & Bayly, P. Mechanics of cortical folding: stress, growth and stability. *Philosophical Transactions of the Royal Society B: Biological Sciences* **373**, 20170321 (2018).

23   De Vincentiis, S. *et al.* Extremely low forces induce extreme axon growth. *Journal of Neuroscience* **40**, 4997-5007 (2020).

24   Katiyar, K. S., Winter, C. C., Struzyna, L. A., Harris, J. P. & Cullen, D. K. Mechanical elongation of astrocyte processes to create living scaffolds for nervous system regeneration. *Journal of tissue engineering and regenerative medicine* **11**, 2737-2751 (2017).

25   Chada, S., Lamoureux, P., Buxbaum, R. E. & Heidemann, S. R. Cytomechanics of neurite outgrowth from chick brain neurons. *Journal of Cell Science* **110**, 1179-1186 (1997).

26   Fass, J. N. & Odde, D. J. Tensile force-dependent neurite elicitation via anti-β1 integrin antibody-coated magnetic beads. *Biophysical journal* **85**, 623-636 (2003).

27   Reillo, I., de Juan Romero, C., García-Cabezas, M. Á. & Borrell, V. A role for intermediate radial glia in the tangential expansion of the mammalian cerebral cortex. *Cerebral cortex* **21**, 1674-1694 (2011).

28   Wang, X. *et al.* Folding, but not surface area expansion, is associated with cellular morphological maturation in the fetal cerebral cortex. *Journal of Neuroscience* **37**, 1971-1983 (2017).

29   Wang, X., Pettersson, D. R., Studholme, C. & Kroenke, C. D. Characterization of laminar zones in the mid-gestation primate brain with magnetic resonance imaging and histological methods. *Frontiers in neuroanatomy* **9**, 147 (2015).

30   Zheng, J. *et al.* Tensile regulation of axonal elongation and initiation. *Journal of Neuroscience* **11**, 1117-1125 (1991).

31   Pfister, B. J., Iwata, A., Meaney, D. F. & Smith, D. H. Extreme stretch growth of integrated axons. *Journal of Neuroscience* **24**, 7978-7983 (2004).

32   Magdesian, M. H. *et al.* Atomic force microscopy reveals important differences in axonal resistance to injury. *Biophysical journal* **103**, 405-414 (2012).

33   Zhang, Y. *et al.* Modeling of the axon membrane skeleton structure and implications for its mechanical properties. *PLoS computational biology* **13**, e1005407 (2017).

34   Costa, A. R., Pinto-Costa, R., Sousa, S. C. & Sousa, M. M. The regulation of axon diameter: from axonal circumferential contractility to activity-dependent axon swelling. *Frontiers in Molecular Neuroscience* **11**, 319 (2018).

35   Yokota, Y. *et al.* Cdc42 and Gsk3 modulate the dynamics of radial glial growth, inter-radial glial interactions and polarity in the developing cerebral cortex. *Development* **137**, 4101-4110 (2010).

36   Vasung, L. *et al.* Structural and Diffusion MRI Analyses With Histological Observations in Patients With Lissencephaly. *Frontiers in cell and developmental biology* **7**, 124 (2019).

37   Im, K., Paldino, M. J., Poduri, A., Sporns, O. & Grant, P. E. Altered white matter connectivity and network organization in polymicrogyria revealed by individual gyral topology-based analysis. *Neuroimage* **86**, 182-193 (2014).

38   Tallinen, T., Chung, J. Y., Biggins, J. S. & Mahadevan, L. Gyrification from constrained cortical expansion. *Proceedings of the National Academy of Sciences* **111**, 12667-12672 (2014).

39   Saito, K. *et al.* Characterization of the Inner and Outer Fiber Layers in the Developing Cerebral Cortex of Gyrencephalic Ferrets. *Cerebral Cortex* **29**, 4303-4311 (2019).

40   Reillo, I. *et al.* A complex code of extrinsic influences on cortical progenitor cells of higher mammals. *Cerebral Cortex* **27**, 4586-4606 (2017).

41   Spedden, E. & Staii, C. Neuron biomechanics probed by atomic force microscopy. *International journal of molecular sciences* **14**, 16124-16140 (2013).

42   Jimenez, V. A. *et al.* Detecting Neurodevelopmental Effects of Early-Gestation Ethanol Exposure: A Nonhuman Primate Model of Ethanol Drinking During Pregnancy. *Alcoholism: Clinical and Experimental Research* **43**, 250-261 (2019).

43 Batchelor, P., Atkinson, D., Hill, D., Calamante, F. & Connelly, A. Anisotropic noise propagation in diffusion tensor MRI sampling schemes. *Magnetic Resonance in Medicine: An Official Journal of the International Society for Magnetic Resonance in Medicine* **49**, 1143-1151 (2003).

44 Yushkevich, P. A. *et al.* User-guided 3D active contour segmentation of anatomical structures: significantly improved efficiency and reliability. *Neuroimage* **31**, 1116-1128 (2006).

45 Van Essen, D. C. *et al.* An integrated software suite for surface-based analyses of cerebral cortex. *Journal of the American Medical Informatics Association* **8**, 443-459 (2001).

6. Acknowledgements

7. Author Contributions

K.G. conceived the hypothesis and developed the mathematical theory and computational models. C.K. and X.W. conceived and designed experimental measures for rhesus macaque. X.W. performed experiments and measurement of DTI data. All authors contributed to interpretation of results. All authors read and edited the manuscript.

8. Competing Interests

The authors declare no competing financial interests.

1   **Supplementary Information**

2

3   **Parameter determination for stress-dependent fiber elongation**

4   In determining parameter, *a*, representing stress-dependent elongation of fibers in the subplate, we considered values

5   from a range of previous experiments and models, as illustrated in Supplementary Table 1.

6   **Supplementary Table 1. Parameter Range for fiber elongation based on available literature**

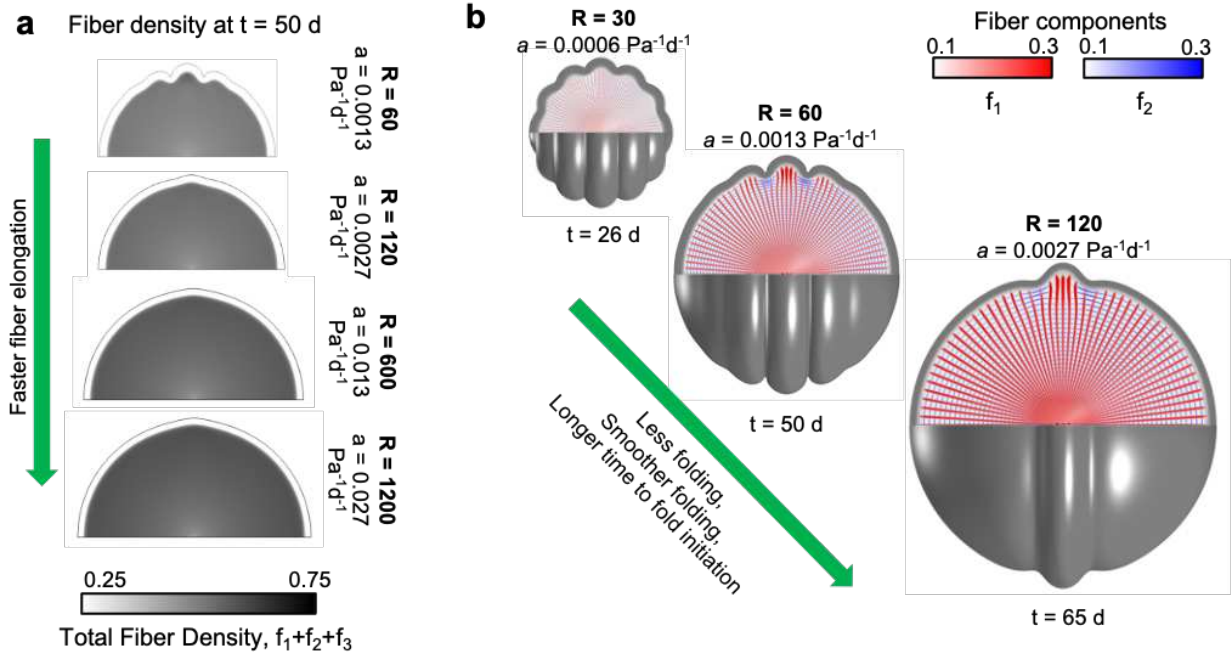| Source	Cell type	Force range, F (pN)	Reported elongation rate, b or G^{axon}	Reported caliber, D (μm)	Estimated rate, *a* ($Pa^{-1}d^{-1}$)	Calculated response ratio, *R*
Katiyar et al. 2017	P0-P1 murine cortical astrocytes	~	0.0125 1/h*	~	0.0001	15
Pfister et al. 2004	Embryonic rat dorsal root ganglia	~	0.076 1/h*	~	0.0004-0.02	91
Holland et al. 2015	Embryonic chick sensory neurons	~	0.08 1/h	~	0.0004-0.02	96
Chada et al. 1997	Embryonic chick forebrain neurons	10-1000	1 μm/μdyne/h	1.0	0.02	850
Fass & Odde 2003	Embryonic chick forebrain neurons	10-1000	1 μm/μdyne/h	1.0	0.02	850
Zheng et al. 1991	Embryonic chick dorsal root ganglia	250-5600	1.5 μm/μdyne/h	2.0	0.1	5,100
Vincentiis et al. 2020	P0-P1 murine hippocampal neurons	<10	0.66 μm/pN/h	5.0	2.1	94,500

7   *Calculated from reported data

8

9   To bring these measures – as well as past model results – into a consistent framework, we considered $R = G^{axon}/g_c$ as

10   a nondimensionalized parameter representing the subplate (fiber) response relative to cortical growth. In this study,

11   the elastic behavior of the subplate is approximated as a nearly incompressible material ($\mu = 300$ Pa, $\kappa = 100\mu$), with

12   fibers growing only in response to axial tension. Under the assumption of an incompressible material undergoing

13   small deformations and uniaxial tension, the stress-strain relationship for model fibers can therefore be

14   approximated as $\sigma = E\varepsilon = 3\mu\varepsilon$, where $E = 3\mu$ approximates Young's modulus of model fibers. Thus, for a given

15   value of *a*, we define $G^{axon} = 3a\mu$ such that $R = G^{axon}/g_c = 3a\mu/g_c$.

1   Using the neurite elongation rates reported for embryonic chick forebrain neurons (Chada et al. 1997), Bayly et al.

2   (2013) roughly approximated a stress-dependent elongation rate constant of $a = 0.003$ Pa^{-1}h^{-1}, leading to $R = 3{,}240$

3   based on approximations described here ($R = 4{,}320$ based on slightly different approximations reported in that

4   study). Alternately, Holland et al. (2015) calibrated a stretch-dependent axon elongation rate of $G^{axon} = 0.08$ h^{-1} and

5   calculated $R = G^{axon}/g_c = 96$. Notably, in models that considered a curved geometry, Bayly et al. (2013) retreated to

6   R values below 10, and Holland et al. (2015) to $R = 32$. This is because, for an enclosed geometry such as a sphere or

7   ellipsoid, faster response R allows subplate growth to keep pace with the growing cortex, dissipating the

8   compressive cortical stresses necessary to induce folding (Supplementary Figure 1).

9   In our final model, we considered a ratio $R = 60$ ($a = 0.0013$ Pa^{-1}d^{-1}, $\mu = 300$ Pa, $g_c = 0.02$ d^{-1}). As shown in

10 Supplementary Figure 1, values as high as $R = 120$ facilitate folding on the same geometry, which is substantially

11 higher than values considered in previous viscoelastic simulations of cortical folding on curved geometries (Bayly et

12 al., 2013; Holland et al., 2015). This discrepancy stems the application of stress-dependent growth in only some

13 tissue components: In our model, growth only occurs in fiber volume fractions, which comprise less than one third

14 of the starting subplate volume, such that net growth of the subplate is slower compared to previous models that

15 apply stress-dependent growth (a) to all subplate tissue.

16 The effects of R on fold morphology agree with previously reported studies (Bayly et al. 2013): As R increases,

17 folds are fewer, smoother, and take longer to appear. In terms of subplate organization, we note that – for all levels

18 of R that induce folding – both sharp and smooth sulci lead to the accumulation of tangential fibers beneath each

19 sulcus. However, the overall density of these tangential components depends on two competing effects: Under

20 slower rates, more sulci develop (polymicrogyria), but tangential fibers have less opportunity for axon elongation

21 (reduced overall fiber density at time of folding). Under faster rates, axons elongate freely, but fewer sulci develop

22 (lissencephaly or pachygyria) that are capable of inducing tangential organization.

1

a Fiber density at t = 50 d

R = 60, a = 0.0013 Pa⁻¹d⁻¹

R = 120, a = 0.0027 Pa⁻¹d⁻¹

R = 600, a = 0.013 Pa⁻¹d⁻¹

R = 1200, a = 0.027 Pa⁻¹d⁻¹

Faster fiber elongation

0.25   0.75

Total Fiber Density, $f_1+f_2+f_3$

b

R = 30
a = 0.0006 Pa⁻¹d⁻¹
t = 26 d

R = 60
a = 0.0013 Pa⁻¹d⁻¹
t = 50 d

R = 120
a = 0.0027 Pa⁻¹d⁻¹
t = 65 d

Less folding,
Smoother folding,
Longer time to fold initiation

Fiber components
0.1   0.3   0.1   0.3
f_1 f_2

2

3 ***Supplementary Figure 1. Effect of stress-dependent fiber elongation rate on folding and subplate organization.***

4 *(a) Effect of faster fiber elongation for a given point in time (T=1, corresponding to 50 gestational days and a 6-*

5 *fold increase in cortical surface area). Faster fiber elongation leads to increased fiber density but reduced folding.*

6 *At extremely high rates, stresses are fully relieved and effect of increasing R plateaus. (b) Fiber organization at the*

7 *onset of folding, considering lower and higher subplate response. Slower rates lead to earlier-forming, sharper, and*

8 *more numerous folds, while faster rates lead to later-forming, smoother, less numerous folds. For all rates that*

9 *induce folding, tangential fibers are observed beneath sulci, but density and location frequency vary.*
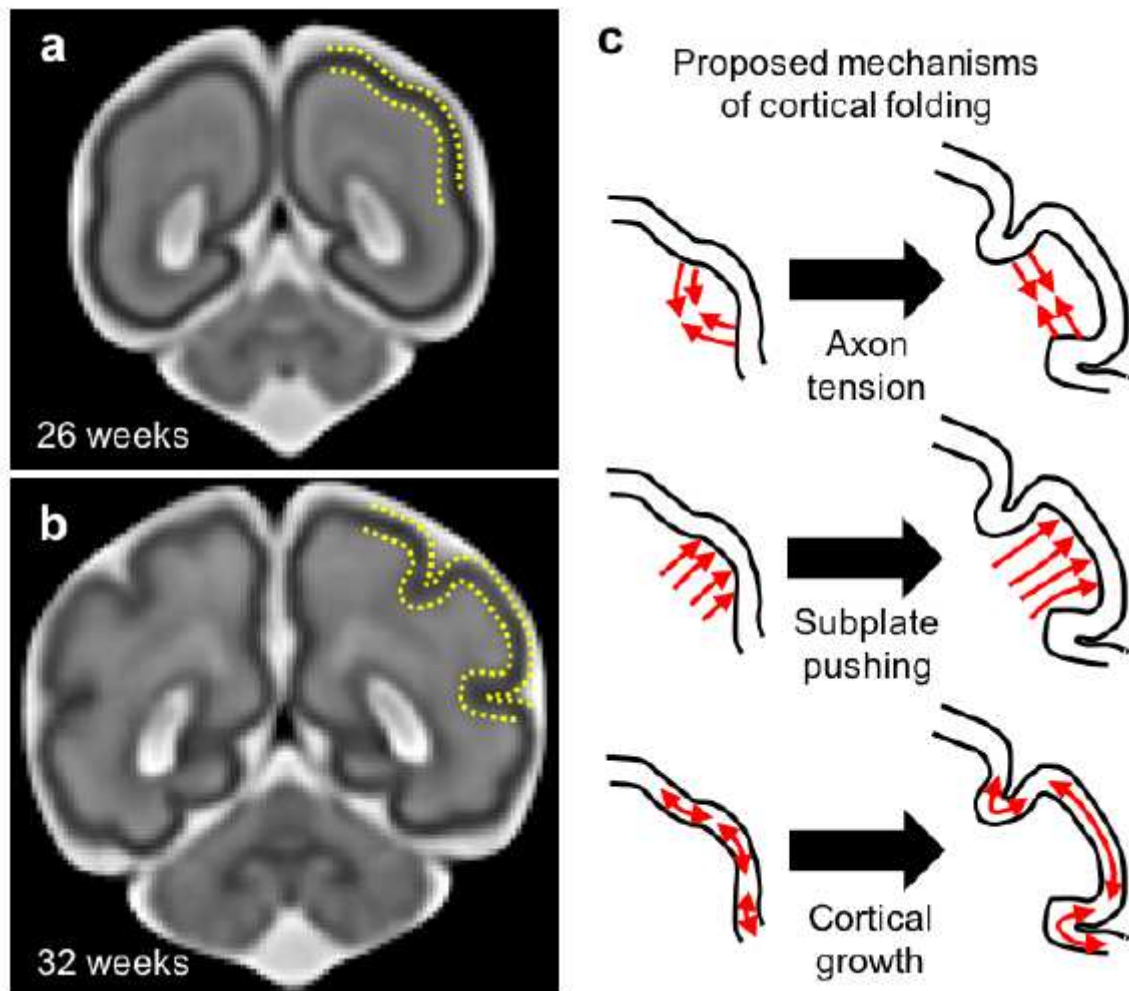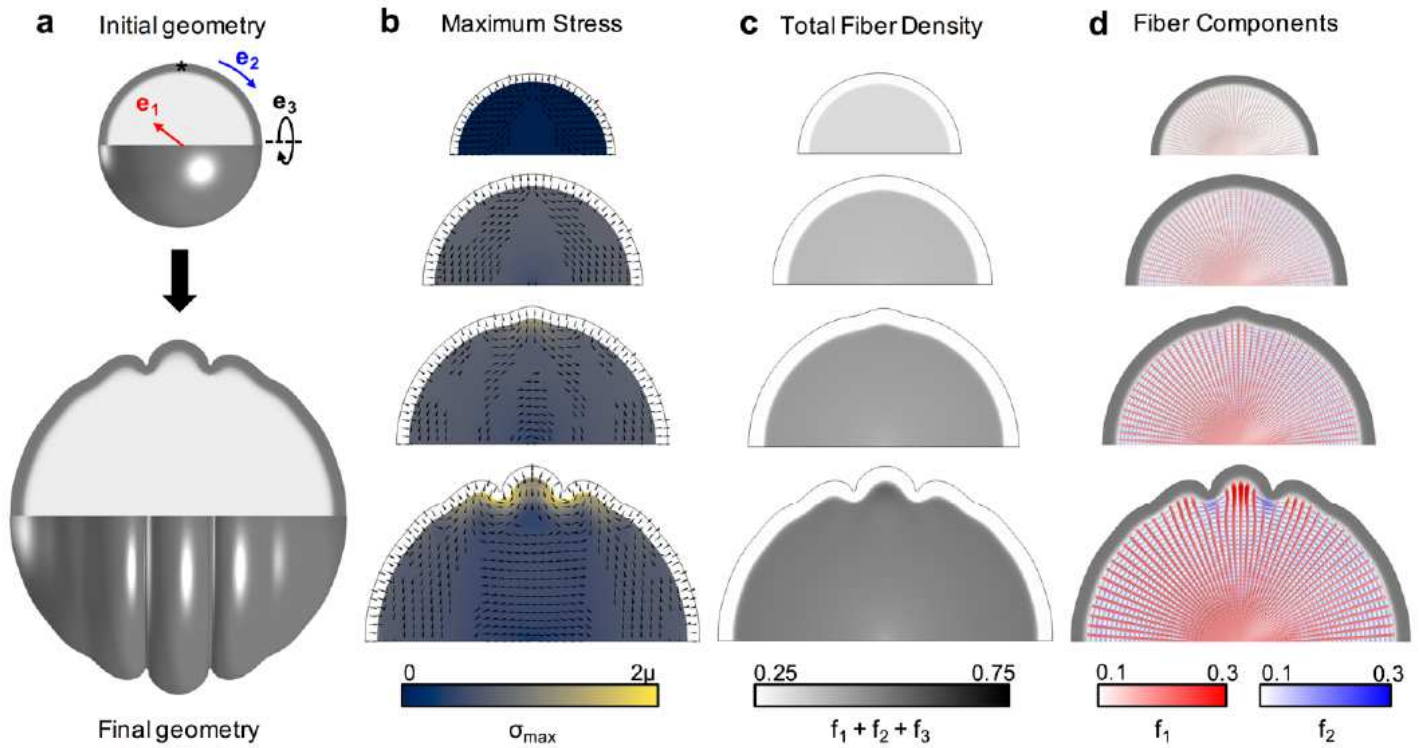
10

11

Figures

Figure 1

Cortical folding and subcortical organization. (a-b) Magnetic resonance images of the fetal human brain at the onset of cortical folding (a) and after formation of cortical folds (b). Magnetic resonance images of the fetal human brain taken from Gholipour et al19. (c) Mechanisms proposed to actively induce cortical folding include axon tension that pulls together specific areas of cortex (top), subplate growth that exerts an outward push to form gyri (middle), and constrained cortical growth that induces mechanical buckling or creasing (bottom).

Figure 2

Tissue remodeling based on mechanical feedback. (a) Expected subplate changes reported over the period of folding. (b) Hypothetical tissue volume element with embedded fibers in initial configuration (left), immediately after stretch (middle), and after fiber growth to relieve tension over a short period of time (right). V0=initial volume, V=current volume, fi=volume fraction of fibers in i-direction. (c) Theoretical
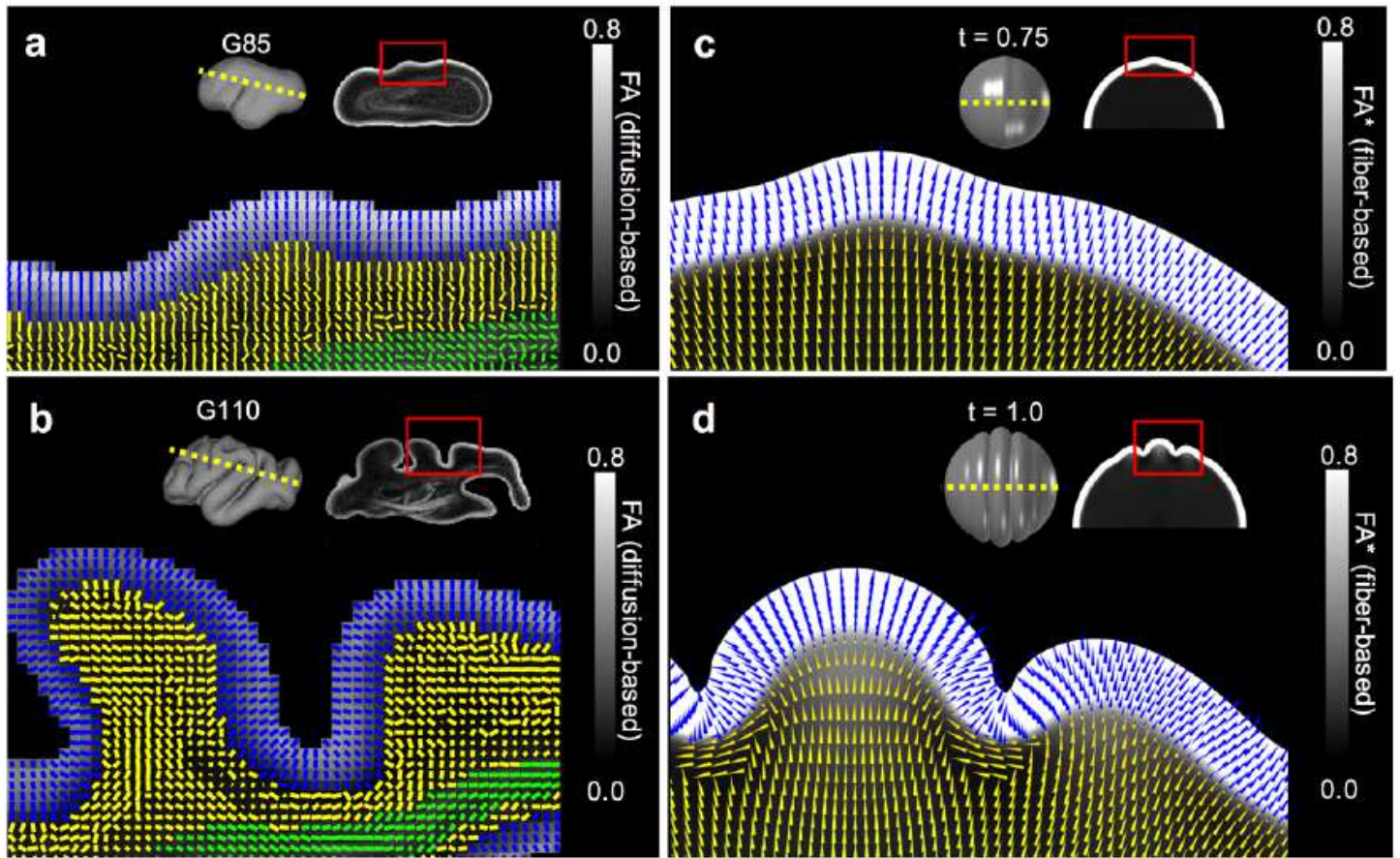
solution for sustained uniaxial tension (σi,0) over time (nondimensionalized such that t*=aσi,0 t), starting from an initial fiber volume fraction of 10%.
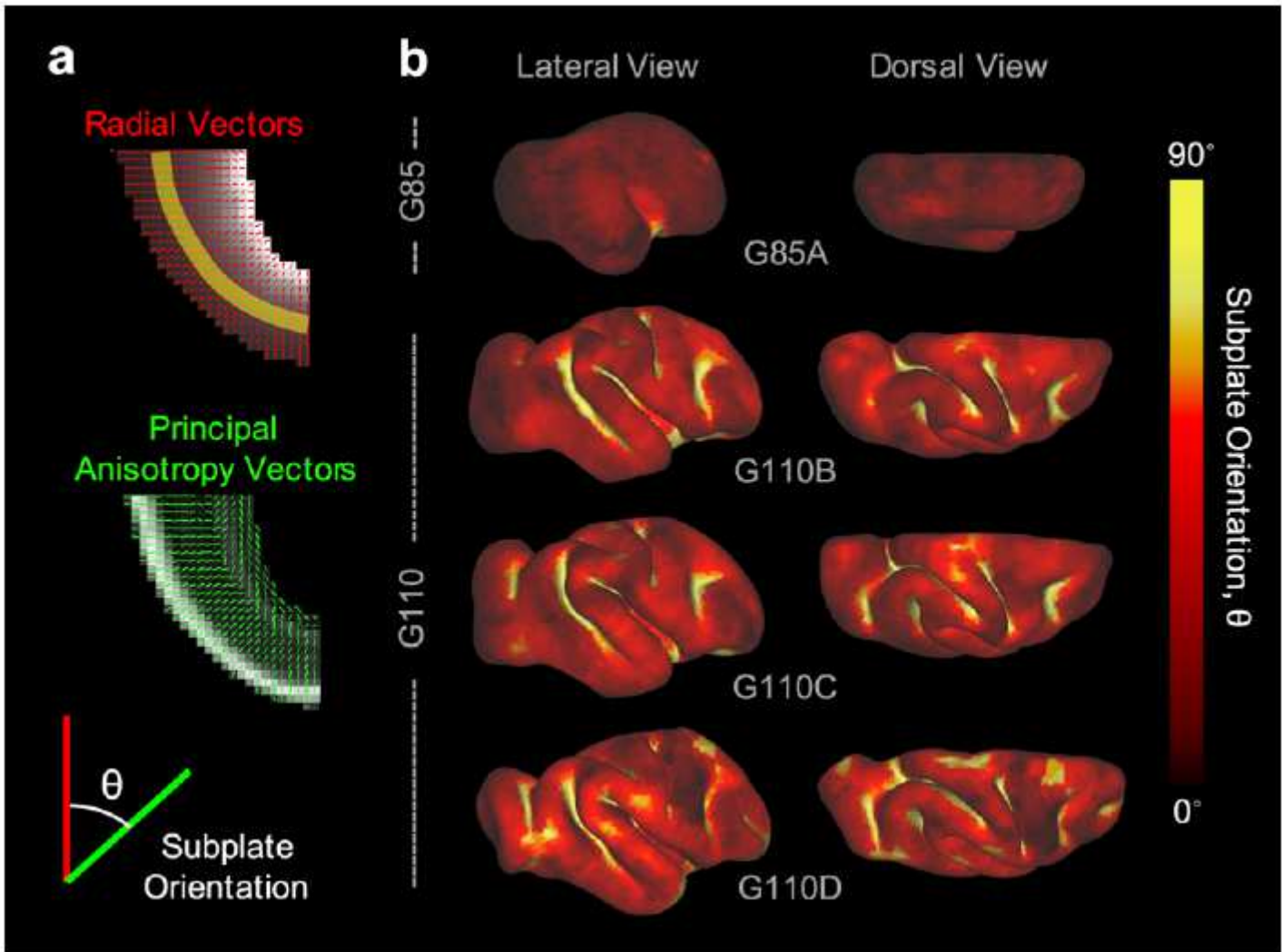

Figure 3

Cortical folding induces stereotyped fiber organization beneath gyri and sulci. (a) Model geometry before and after folding. For the axisymmetric model, material coordinate directions are defined in radial (e1), circumferential-tangential (e2), and axisymmetric-tangential directions (e3), and can be followed over the course of deformation. Asterisk denotes location of symmetry-breaking perturbation. (b-d) Evolution of maximum nondimensionalized Cauchy stress (tension), total fiber density, and directional fiber components in the subplate over the course of folding (from top to bottom, simulation time T=0, 0.5, 0.75, 1). In (d), fiber volume fraction in a given direction is represented by both color and line thickness.
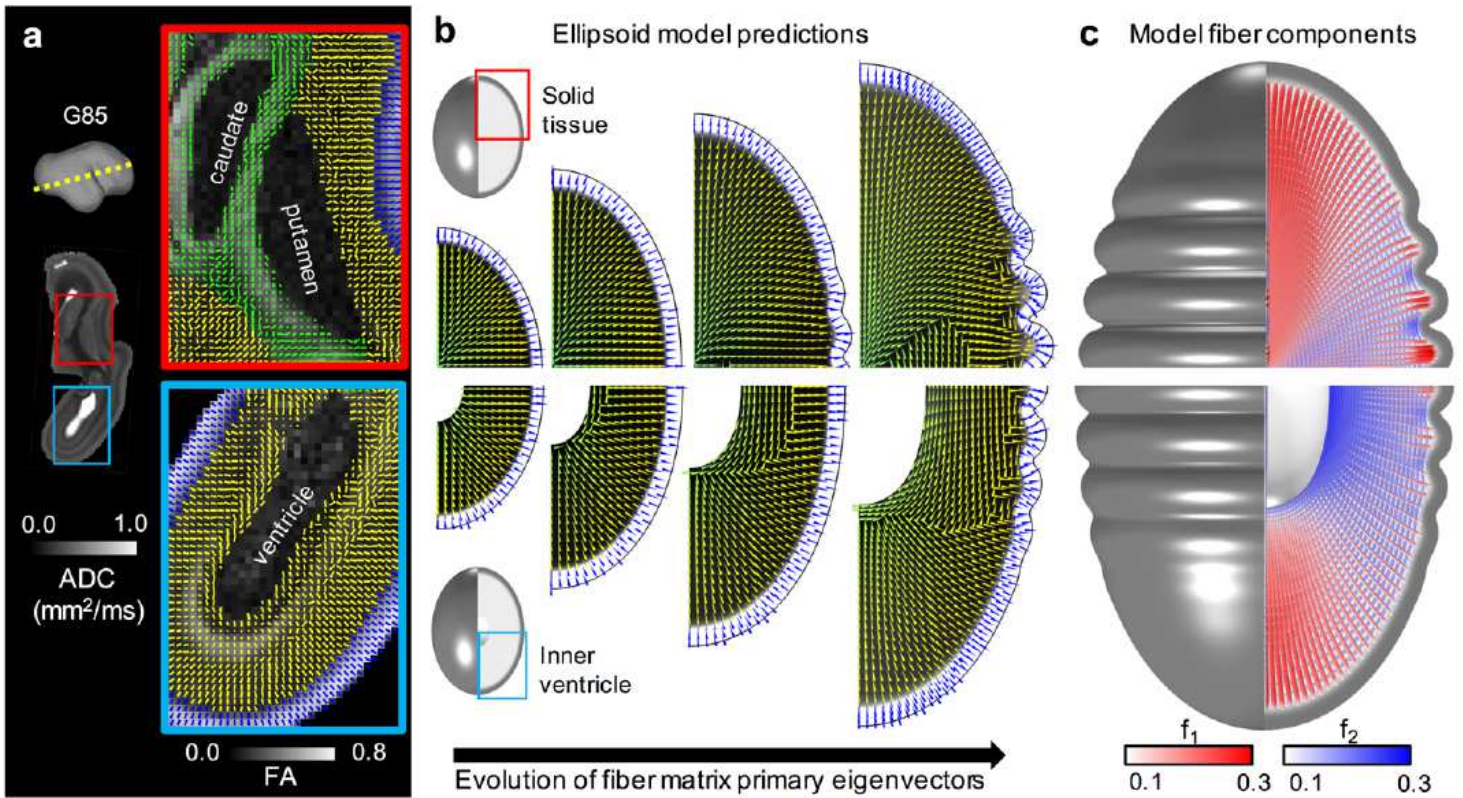
Figure 4

Anisotropy in the developing subplate matches model predictions. (a-b) Primary eigenvector directions (tick marks) based on high-resolution DTI of the rhesus macaque brain at G85 (a) and G110 (b), at the slice indicated by the yellow dotted line and location indicated by the red box. Fractional anisotropy (FA) maps are shown as an underlay. (c-d) Primary eigenvector directions (tick marks) based on the fiber volume fractions predicted by our model at the onset of folding (c) and after fold formation (d). FA* maps are based on the 3D tensor describing model subplate volume fractions, with cortical FA* (not defined in model) set to 1 for visualization. Tick marks are colored such that blue=cortex, yellow=subplate, green=deeper subcortical layers.

Figure 5

Primary anisotropy orientation across subplate in developing rhesus macaque. (a) Radial orientation vectors generated from a gradient representing distance from the cortical surface (red), and primary eigenvectors generated from DTI (green). For voxels at a set distance from the cortical surface (illustrated by yellow strip), subplate orientation angle was calculated as the angle between the radial (red) and principal anisotropy (green) vectors. (b) Subplate orientation angle mapped onto cortical surface reconstructions for one G85 (top) and three individual G110 (bottom) brains. Panel (a) modified from Wang et al29.

Figure 6

Stresses predict accurate trends with respect to deep fiber tracts. (a) Primary eigenvector directions (tick marks) based on high-resolution DTI of the rhesus macaque brain at G85 at the slice indicated by the yellow dotted line and locations indicated by the red and blue boxes (ADC map shown to visualize deep gray matter structures). For maps showing primary eigenvector directions, fractional anisotropy (FA) maps are shown as an underlay. Tangential orientation is visible along the ventricle prior to folding. (b) Primary eigenvector directions (tick marks) based on the fiber volume fractions predicted by ellipsoidal models with solid core of tissue (top) and open inner ventricle (bottom). (From left to right, T=0, 0.5, 0.75, 1.) FA* underlay is based on the 3D tensor describing volume fractions in our model (see Materials and Methods for details). Tick marks are colored such that blue=cortex, yellow=subplate, green=deep brain structures. (c) Directional fiber components at T=1, with fiber volume fraction in a given direction represented by both color and line thickness. On an ellipsoidal geometry, tangential fibers accumulate first and in greater magnitude along the longer axis, both along the ventricle and in intermediate layers.